PERGAMON

Journal of Structural Geology 24 (2002) 773–782

JOURNAL OF STRUCTURAL GEOLOGY

www.elsevier.com/locate/jstrugeo

A new technique for 3-D flexural-slip restoration

Paul Griffiths[a], Serena Jones[a,*], Neil Salter[b], Frauke Schaefer[c], Robert Osfield[d], Herbert Reiser[e]

[a]*Midland Valley Exploration Ltd, 14 Park Circus, Glasgow G3 6AX, UK*
[b]*Cisco Systems, Cumbernauld, Glasgow G68 9LE, UK*
[c]*Bundesanstalt für Geowissenschaften und Rohstoffe, Stilleweg 2, 30655 Hannover, Germany*
[d]*29 Hamilton Way, Prestwick, Ayrshire KA9 1BJ, UK*
[e]*BEB Erdgas und Erdoel Gmbh, Riethorst 12, D-30659 Hannover, Germany*

Received 17 August 2000; revised 7 February 2001; accepted 25 April 2001

Abstract

A new flexural-slip structural restoration technique for three-dimensional (3-D) digital models has been developed. This technique utilises a slip method that preserves volume in 3-D, line length in a given unfolding direction (of a specified surface and of layers parallel to this surface), and orthogonal bed thickness. These constraints enable the restoration of 3-D fault-propagation, fault-bend and detachment folds.

The 3-D model is comprised of objects such as interpreted horizon and/or fault surfaces that are created from irregular, triangulated meshes. For a given model, a parallel sinuous-slip system is calculated from the geometry of a specified template surface and from a fixed pin surface that passes through all vertices of the triangulated meshes in the specified folding direction. The entire slip system then is folded to a new shape, which is defined by a geometric surface that can be curved or planar. In doing so, all vertices within the system are transformed to their new locations to generate a newly-folded 3-D model.

We demonstrate the 3-D restoration technique by using a case study of an evaporite-cored contractional fold in the NW German Basin. Our restorations depict the 3-D sequential growth of the fold from 146 Ma through late Mesozoic time, and show that the shortening direction was towards NNE with the main contractional phase initiating during the late Cretaceous.

Keywords: Flexural-slip restoration; Digital model; Triangulation meshes

1. Introduction

A number of techniques have successfully been applied to cross-section and surface restoration of contractional folds (e.g. Geiser et al., 1988; Williams et al., 1997; Hennings et al., 2000). These techniques have been used to study detailed contractional fold geometries and their associated strains. While insightful, these methods require that cross-sections be treated independently and that structural surfaces be unfolded separately. This paper describes a new three-dimensional (3-D) flexural-slip restoration algorithm, which allows the restoration of multiple, geometrically-complex, and non-parallel surfaces within a 3-D digital model in a single modelling increment. This plane-strain algorithm also preserves the connectivity of parallel or non-parallel surfaces using a defined slip system.

To illustrate the method and its flexibility as well as to qualify the enhanced understanding obtained from using this 3-D flexural-slip approach during geometric modelling, we restored and analysed a folded structure in the NW German Basin. Due to the 3-D nature of the algorithm, the unfolding direction becomes an important parameter that affects the results of our case study. For this reason, an approach for defining the optimum unfolding direction is also described in relation to this study.

2. The 3-D flexural folding technique

2.1. Model representation

The folding technique utilises a digital geological model that consists of 3-D surfaces, which may represent any geological surface (e.g. faults and/or stratigraphic horizons). These surfaces, in turn, are composed of sets of data points or nodes that are connected to form arrays of regular or irregular triangles (neighbouring triangles may or may not have identical orientations). The data structure of the digital model uniquely identifies each node and retains its connection information to other nodes in the surface. This information allows the triangle connectivity (or object topology)

* Corresponding author. Tel.: +44-141-332-2681; fax: +44-141-332-6792.
E-mail address: serena@mve.com (S. Jones).

0191-8141/02/$ - see front matter
PII: S0191-8141(01)00124-9

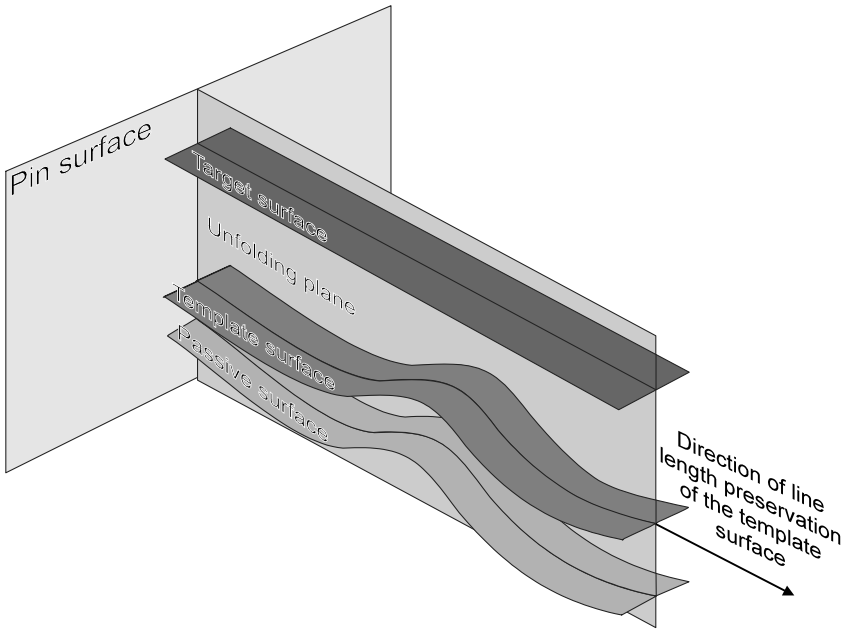

Fig. 1. Components of the flexural-slip folding technique. The template surface defines the initial slip system geometry. The target surface defines the final slip system geometry. Passive surfaces are carried with the template surface as it is deformed with the flexural-slip algorithm. The pin surface defines the surface of zero slip during the folding process. The intersection line of the unfolding plane and the template surface defines the folding direction in which the line length of the template surface is maintained.

to remain the same before and after folding. That is, the way the triangles are connected to one another is maintained throughout the restoration. In addition to triangulated surfaces, the model may also include 3-D polylines that are composed of connected line segments, and arrays of nodes connected to form volumes that are represented as tetrahedral elements. Although we describe our algorithm using nodes, the technique is generic and may therefore be carried out on any object within the digital model (e.g. surfaces, 3-D polylines and tetrahedral volume elements).

2.2. Slip system determination

The folding technique is based on the transformation of a flexural-slip system from a folded or flat geometry (template surface) to another folded or flat geometry (target surface). To determine the slip system, a number of model components are required (Fig. 1):

1. The template surface, which is a triangulated mesh, may be a folded (including overturned geometries) or planar surface. The geometry of the template surface defines the initial slip system geometry.
2. The target surface, which is either a triangulated mesh or a mathematical plane, may be a folded (including overturned geometries) or planar surface. The geometry of the target surface defines the final geometry of the slip system.
3. The pin surface, which is either a triangulated mesh or a mathematical plane, may be a geometrically complex or planar surface. The pin surface defines the surface of zero slip during the folding process. Nodes of geological surfaces that intersect this pin surface will not slip during folding. However, a node on the pin surface pre-folding may be translated to another location on the pin surface post-folding.
4. The unfolding plane is a vertical mathematical plane. Nodes are displaced parallel to the unfolding plane as they move along the slip system, relative to the pin, the template surface, and the target surface.

In addition to the template surface, other objects may be deformed during the folding process (these objects are called passive objects). Passive objects may be any node-based geometric objects (e.g. polylines, triangulated surfaces or tetrahedral volumes). They are folded on a per-node basis parallel to the defined slip system.

We calculate the initial slip system based on the geometry of the template surface and the direction of the unfolding plane. The algorithm passes a vertical slice that is parallel to the unfolding plane through *each node* within the 3-D model, and the intersection line of the vertical slice with the template surface is calculated. Dip-domain boundaries for the template intersection line are then calculated (Fig. 2). This defines the geometry of the slip system for that particular node. This procedure is then iteratively applied to each node on the geological objects selected to be unfolded to the target geometry. This procedure simulates flexural flow (Ramsay and Huber, 1987) parallel to the template surface. Any other geological surface behaves as a passive marker that does not experience flexural slip along its layering. The exceptions, of course, are layers that behave

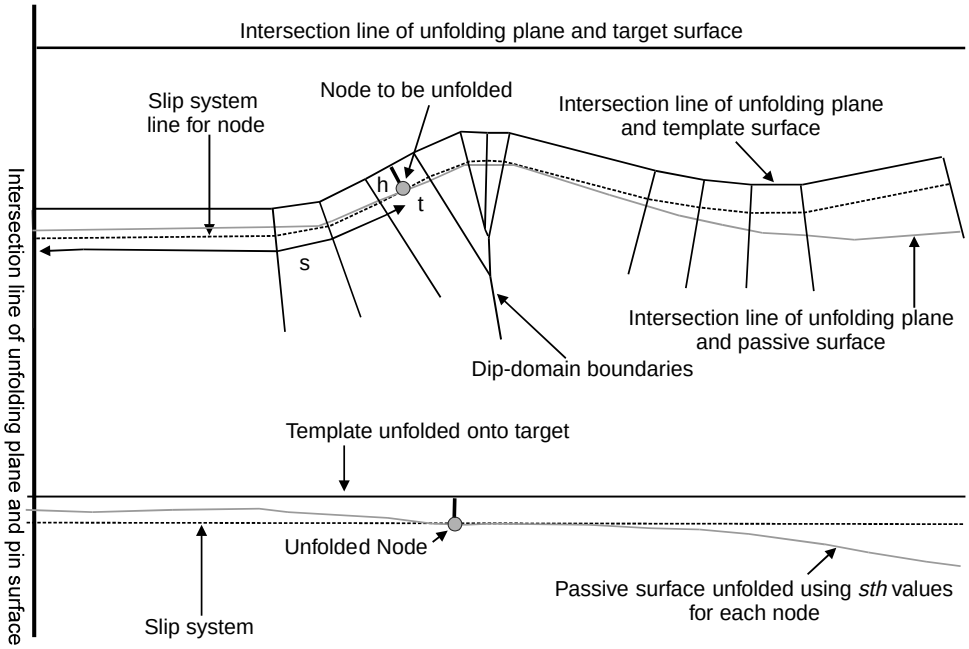

Fig. 2. Node-based slip system determination and folding process. Slip system values are determined for each node to be deformed. A vertical slice in the orientation of the unfolding plane through the node is calculated. The slip system through the node is defined parallel to the intersection line of the template surface and the unfolding plane. From this, the node values in the slip system, *s*th, are determined. The node is transferred to the new position by maintaining the *s*th values for the node transformation.

as parallel folds with respect to the template surface. These then effectively are deforming by flexural slip parallel to their layering. The final slip system is calculated based on the geometry of the target surface using a similar procedure (Fig. 2).

The folding algorithm preserves several aspects of the 3-D model: (1) line length of the template surface in the orientation of the unfolding direction, (2) line lengths of surfaces parallel to the template surface in the unfolding direction, (3) thickness orthogonal to the template surface, (4) volume of the folded objects, and (5) cross-sectional area in the orientation of the unfolding direction. These constraints are maintained whether there is constant or variable shortening along the strike of a fold.

2.3. Flexural restoration process

Once the slip system has been defined, each object (i.e. the template surface and the passive objects) is systematically restored. The initial position of each node within each object is determined by its relative position with respect to the template surface, the unfolding plane and the position of the node along the sinuous length of the slip system. The nodal positions are defined by the *s*th local coordinate system (Fig. 2):

s: The distance from the node to the pin surface as measured along the node's slip system line. This sinuous distance is defined by the intersection of the template surface and a vertical slice through the node parallel to the unfolding plane (Fig. 2).

t: The orthogonal distance of the node from an arbitrary, fixed position vertical unfolding plane (i.e. in and out of the page in Fig. 2). The *t* value forms a relative 3-D coordinate system that retains on which vertical slice a given node is located.

h: The orthogonal distance of the node from the template surface. This distance is defined by the intersection of the template surface and the unfolding plane at the location of a node (Fig. 2). All nodes are located within a dip domain as dip-domain boundaries are defined as being infinitely thin.

This *s*th value for the node defines where the final folded position of the node lies within the target slip system. To calculate this final position, the slip system for the target surface is calculated the same way as for the template surface. The node is placed within the target slip system such that the values for *s*, *t* and *h* are maintained, thus defining its new geometry (Fig. 2).

2.4. Benefits of the restoration technique

The key difference between this technique and previous flexural unfolding methodologies is that object restoration is performed on a per-node basis while maintaining the node connectivity during the folding process. Previous techniques using triangulated surfaces divided the surfaces into separate triangles, unfolded each triangle to a datum, and then packed the triangles together using a fitting algorithm (e.g. Gratier et al., 1991; Gratier and Guillier, 1993; Williams et al., 1997; Rouby et al., 2000). These processes required that

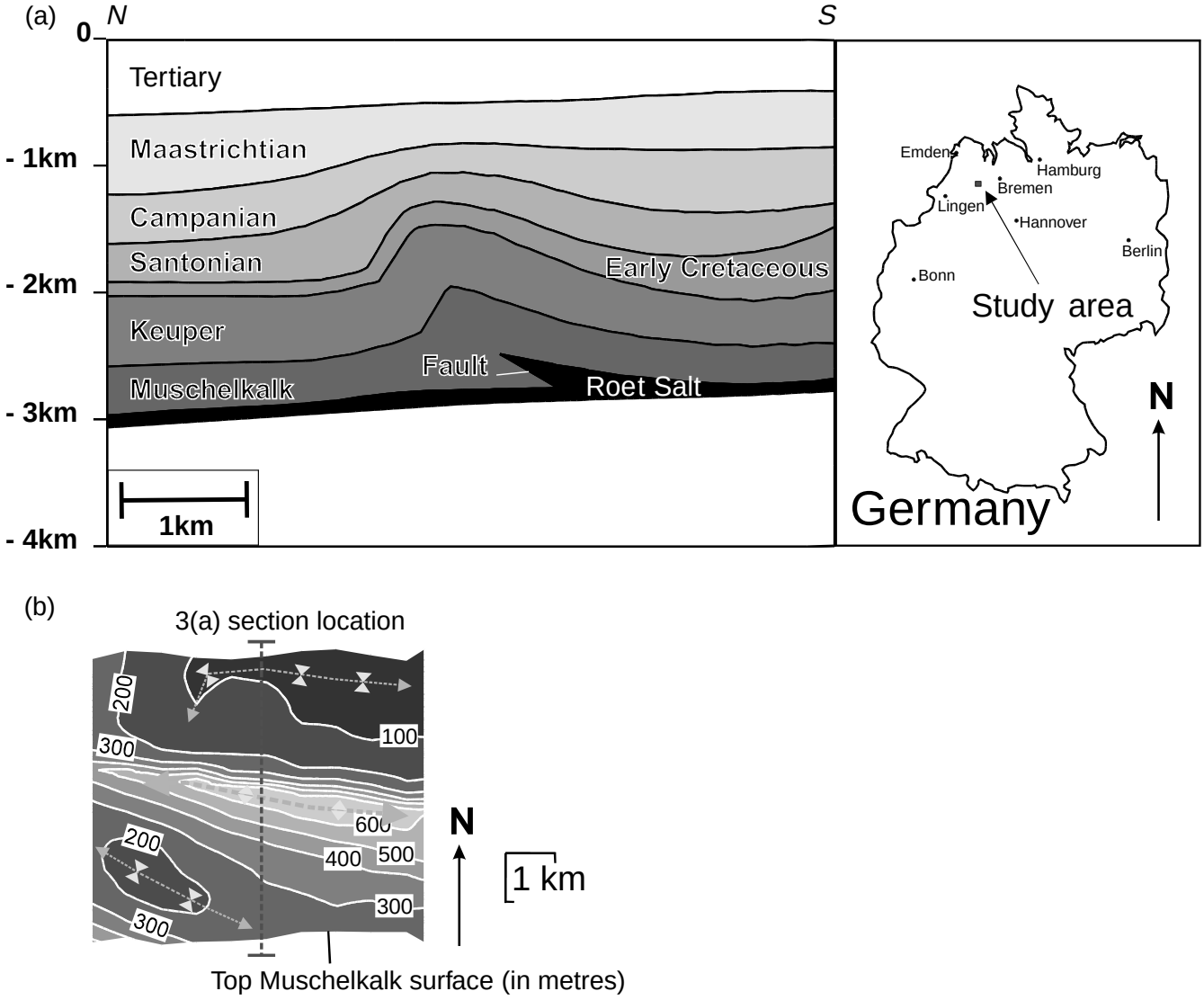

Fig. 3. Present-day geometry of the contractional fault-related fold from the NW German Basin. (a) Cross-section, with 0 m datum representing sea level, showing a representative geometry of the structure. Inset map illustrates the study area location of the fold. (b) Map showing the present-day relative structural relief of the Top Muschelkalk surface and the location of cross-section in (a). The contour interval is 100 m and relative to the lowest point on the surface in order to emphasise the relative structural relief. Arrows are used to highlight the fold axes, including the relatively minor synclinal features.

each surface be unfolded separately, without explicitly preserving volume or maintaining flexural-flow linkage between the surfaces. In contrast, our restoration technique maintains node connectivity throughout the restoration, allowing volumes containing multiple surfaces to be restored in a single operation. Because the technique does not require triangle fitting, strains that are generated during the restoration process can be analysed in a geological context. Our technique also provides advantages over previous inversion schemes for searching for an optimal transformation from one folded state to another (e.g. Leger et al., 1997). Specifically, the calculated slip system explicitly preserves: (1) line length in the orientation of the unfolding plane of the template surface; (2) thickness orthogonal to the slip system; (3) line length in the unfolding direction of surfaces parallel to the template surface; and (4) volume of the folded objects.

3. Application of the restoration technique

We test our restoration technique on a contractional fold in the NW German Basin. The structure is located near the northern margin of the Jurassic to early Cretaceous Lower Saxony Basin, which has been inverted during late Cretaceous times (Baldschuhn et al., 1991; Kockel et al., 1994; Fig. 3a). Inversion is manifested by thrusting and thrust-related folding through the reactivation of former basin-bounding normal faults and by exploiting Permo–Triassic halite layers as detachment horizons.

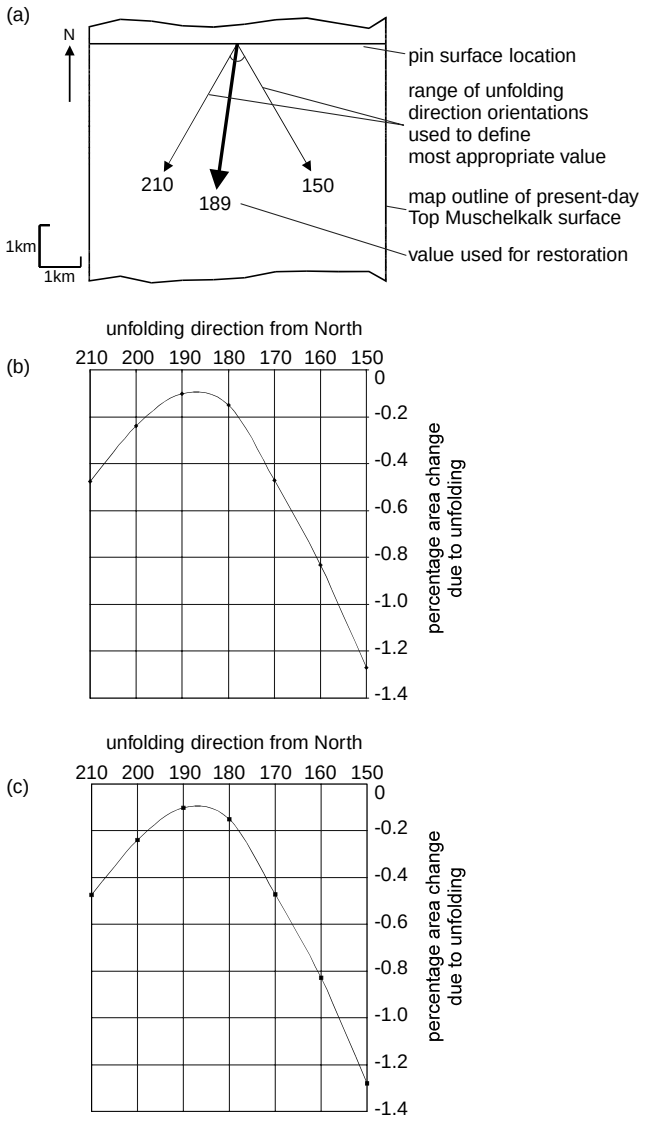

Fig. 4. Unfolding direction sensitivity analysis. (a) Map outline of the present-day Top Muschelkalk surface with the range of unfolding directions used to determine the most appropriate unfolding direction. (b) Plot of the percentage area change due to unfolding versus unfolding direction from north. The pin surface was oriented E–W. (c) Plot of the percentage area change due to unfolding versus unfolding direction from north. The pin surface was oriented orthogonally to the unfolding plane orientation. Note that this plot is almost identical to (b) with the implication that the unfolding strain is insensitive to the pin surface orientation.

The model used for this study was built from a depth-converted, 3-D seismic interpretation of the structure, based on unpublished hydrocarbon exploration data, kindly provided by BEB Erdgas und Erdöl GmbH. Well data also help constrain the interpretation and the depth conversion process. The model is approximately 6 km by 6 km in map extent, and 3 km in depth. It contains eight surfaces that represent interpreted seismic horizons of different geological surfaces. From oldest to youngest they are: the Base Roet; Top Roet; Top Muschelkalk; Base Cretaceous; Near Base Cretaceous; Top Santonian; Top Campanian; and Base Tertiary (Fig. 3).

Strata beneath the Roet halite/anhydrite layer contain lower Triassic terrestrial sandstones with intercalated claystones and siltstones (Kockel et al., 1994). Above the Roet interval, the middle Triassic Muschelkalk is comprised of shallow marine limestones with minor salt intercalations, whereas the upper Triassic Keuper sediments are continental claystones that contain some minor salt layers. The Jurassic interval is interpreted to be missing, probably reflecting the structure's location immediately adjacent to, but outside the actual, Lower Saxony Basin. Jurassic sediments either were not deposited or were eroded from the flanks of the basin. A few kilometres south of the study area, the Jurassic interval is characterised by a succession of marls, claystones, and minor sandstones of marine to deltaic facies. These strata are overlain by early Cretaceous marine deposits with marls, claystones, and sandstone intercalations. Within the region of interest, the early Cretaceous interval is condensed compared with the actual Lower Saxony Basin to the south, which shows thickening towards the centre of the basin (Fig. 3a). Late Cretaceous strata are dominated by Santonian, Campanian, and Maastrichtian marl deposits. Marine deposition continued on into the Tertiary with strata being predominately claystones (Kockel et al., 1994).

The actual structure may be described as an asymmetric, thrust-cored fold with thickness variations within most of the stratigraphic layers involved (Fig. 3). At the base of the interpretation, the early Triassic Base Roet surface dips slightly to the north; elsewhere the Triassic Roet evaporite layer is folded along and is offset by a thrust fault (which strikes ESE–WNW parallel to the overlying folds). The overlying Triassic-age Keuper layer is folded and shows thinning to the south (Fig. 3a). Early Cretaceous strata also display thickness changes, but with thinning to the north. Above the early Cretaceous layer, the late Cretaceous units are all folded with thickness changes across the fold axis, whereas the overlying Tertiary is regionally dipping to the north and is not folded.

The lowermost folded, but unfaulted, horizon is the Top Muschelkalk surface; it has a structural relief of over 600 m (Fig. 3b). The surface is deformed into an anticline with an E–W doubly-plunging axial trace that trends towards 098°.

3.1. Restoration methodology

The object of the restoration was to examine the temporal evolution of the fold. In performing the 3-D restoration, we assume that the structure grew as a fault-propagation fold that deformed by flexural-slip/flexural-flow. We first sequentially decompacted the 3-D surfaces and then unfolded them to a horizontal datum using a vertical planar pin surface placed in the foreland of the fold. The 3-D decompaction utilised North Sea compactional values for the appropriate sedimentary units (Allen and Allen, 1990).

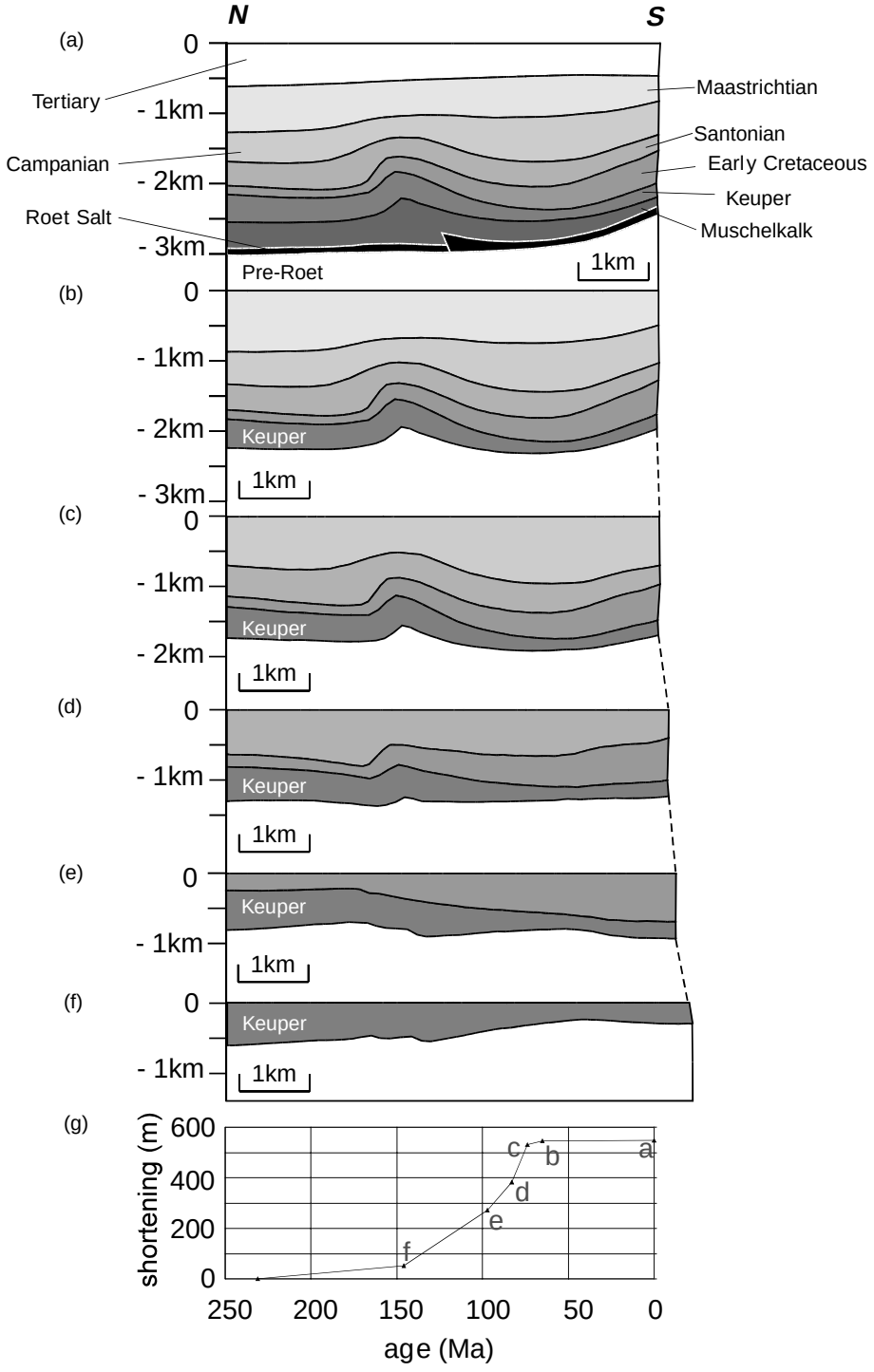

Fig. 5. Sequential palinspastic sections extracted from the restored 3-D models depicting the structural evolution of the fold. Sections were extracted from the 3-D model parallel to the maximum shortening direction (189°). The cross-sections have no vertical exaggeration. (a) Present-day geometry. (b) Restoration of the Base Tertiary surface. (c) Restoration of the Top Campanian surface. (d) Restoration of the Top Santonian surface. (e) Restoration of the Near Base Cretaceous (or 'Base Santonian') surface. (f) Restoration of the Base Cretaceous surface. (g) Plot of shortening versus geological age taken from restorations shown in (a)– (f). Age data are based on Harland et al. (1989). Note that the absolute age for the 'Near Base Cretaceous' horizon has been taken to represent the Base Santonian (97 Ma).

At each restoration stage, the uppermost stratigraphic surface was unfolded to the datum whilst the underlying surfaces were carried as passive objects. The underlying layers were sequentially unfolded as the restoration proceeded. Horizons below the Top Muschelkalk have not been restored in this analysis as it seemed inappropriate to restore faulted layers that involved evaporites using a flexural-slip mechanism (however, in general, faulted

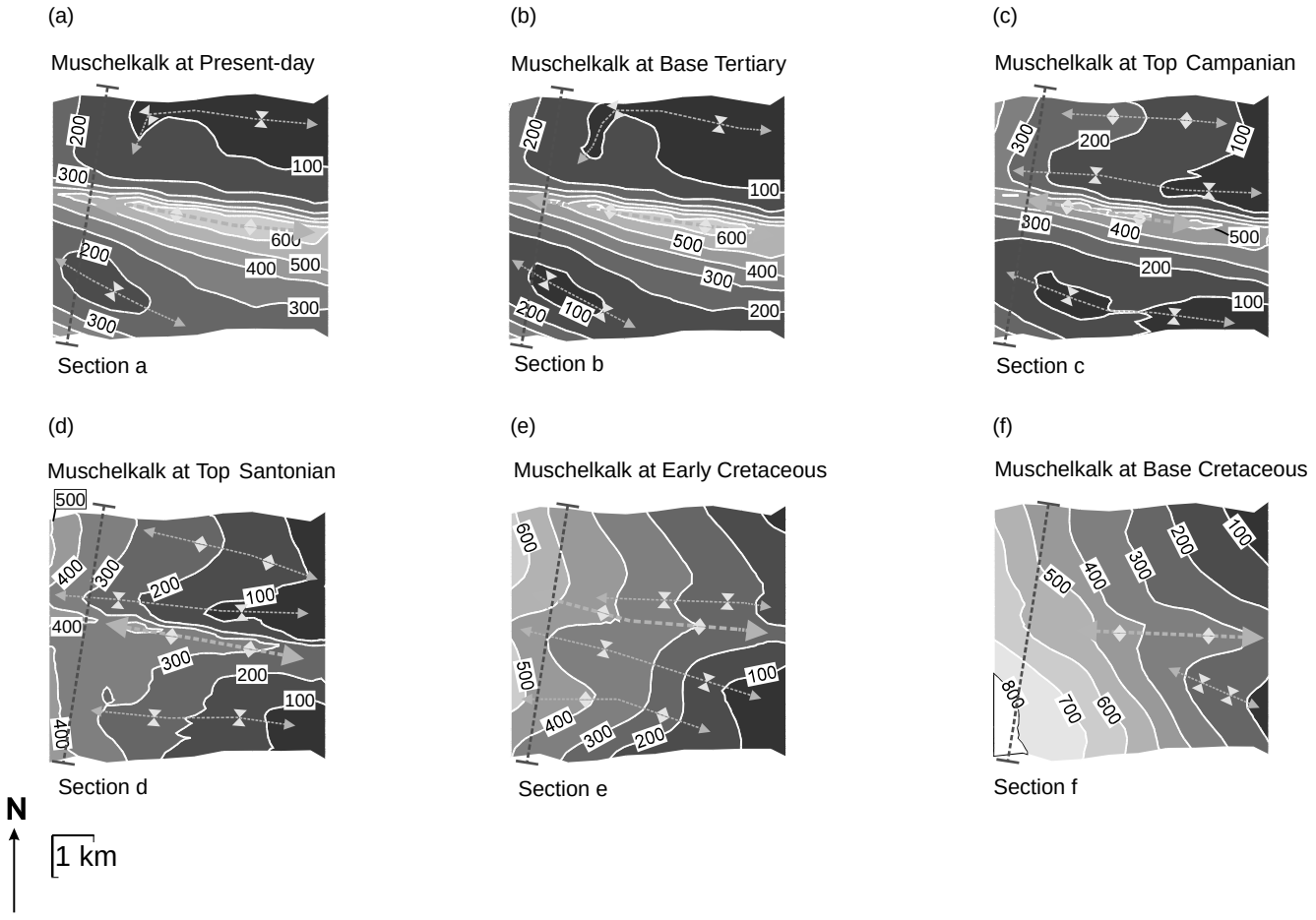

Fig. 6. Structural-relief maps of the Top Muschelkalk surface at each stage of the 3-D restoration. Contours are relative to the lowest point on each horizon to show the comparative size of the folds through geological time. The darker shades show the lowest areas on each surface, whereas the lighter shades are the highest regions. Contour interval is 100 m. Cross-section locations refer to the palinspastic sections in Fig. 5. Arrows are used to highlight the fold axes, including the relatively minor features.

horizons and fault surfaces may be restored using our restoration approach).

3.2. Sensitivity testing of unfolding direction for 3-D restoration

To determine the most appropriate unfolding direction and pin surface orientation for the restorations, two analyses were performed using the present-day Top Muschelkalk surface (Fig. 4). The first analysis was designed to test the sensitivity of total surface area change with variation of the unfolding plane orientation. We assumed that the most appropriate unfolding plane orientation will result in the minimum surface area change. The first analysis maintained a pin surface orientation of 090° (E–W), whilst the unfolding plane orientation was varied (Fig. 4b). The second analysis tested the sensitivity of the total surface area change to the pin surface orientation. In this analysis the pin surface was kept orthogonal to the unfolding plane as the unfolding plane orientation was varied (Fig. 4c).

The difference in percentage area change of the surface by using a constant or an orthogonal pin surface orientation appears to be negligible compared with the area variation due to the change in unfolding plane azimuth. This suggests that the unfolding process is not sensitive to the pin surface orientation (Fig. 4b and c). It is possible to automate the determination of the most appropriate unfolding orientation by analysis of the surface shape; however, a description of this method is beyond the scope of this paper.

The optimal unfolding direction based on minimising the surface area change was determined to be 189°. This orientation has been used throughout all the restoration stages. In addition, the pin surface orientation was kept at a constant 090° (E–W) orientation for all restorations.

3.3. Restoration results

The restoration results are presented from present-day to the earliest Cretaceous, which is the order of the restoration sequence (Figs. 5 and 6). The geological interpretation has been restored through six unfolding stages (Figs. 5 and 6). The section illustrated in Fig. 5 is representative of the

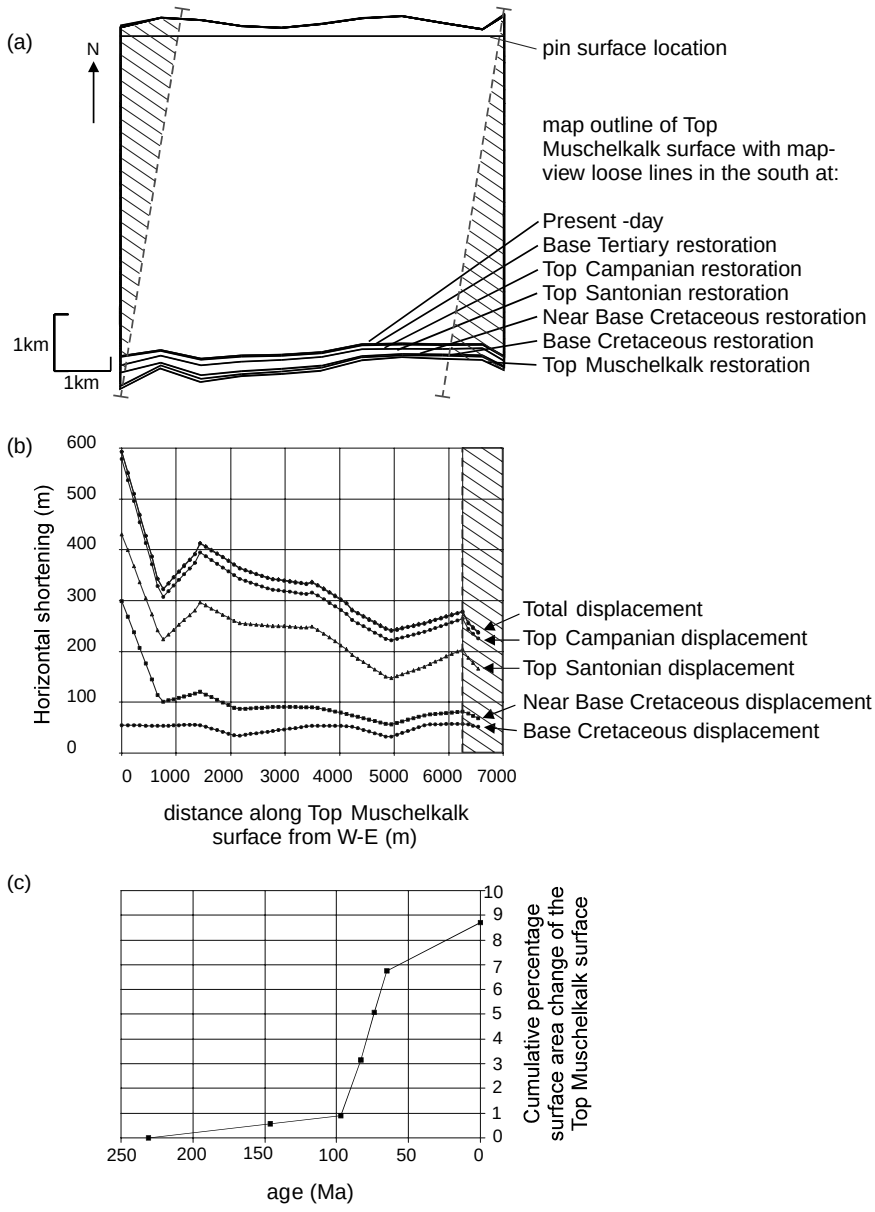

Fig. 7. Analyses of the shortening and area strain at Top Muschelkalk level based on sequential restorations. (a) Map of the outlines of the Top Muschelkalk surface at each restoration stage. The southern margin of each surface represents the loose line from each restoration. (b) Plot of horizontal shortening versus distance along the Top Muschelkalk surface from west to east. Lines on the plot show the variation in shortening at Top Muschelkalk level at each stage of the restoration. (c) Plot of cumulative percentage area change for the Top Muschelkalk surface versus geological age. The plot illustrates the accumulation of strain from the undeformed to the present-day shape of the Top Muschelkalk surface.

evolution of the structure through time parallel to the maximum shortening direction (189°). Decompaction at each restoration stage has produced an increase in volume (and hence cross-sectional area) of the structure as layers were backstripped (Fig. 5).

By comparing the present-day palinspastic maps and cross-sections with their latest Cretaceous counterparts, the structural-relief contours at Top Muschelkalk level are very similar (Figs. 5a and b and 6a and b). The interpretation of the similarity of the maps is that during Tertiary times, there was very little growth of the folds (Fig. 5g). However, regional tilting to the north did occur during this time.

The restorations to latest Cretaceous times (Maastrichtian and Campanian deposition) show the progressive growth in amplitude of the anticline and flanking synclines, coupled with continued shortening (Figs. 5b and c and 6b and c). In particular, the anticline grew in amplitude and broadened in the east. The growth of the fold is represented by thickness changes in the Maastrichtian and Campanian layers.

The latest Santonian restoration (83 Ma) suggests at Top Muschelkalk level the initiation of the fault-propagation fold (Figs. 5d and 6d). The regional dip of the Top Muschelkalk surface during Santonian times was towards the ESE. The majority shortening that produced the

fault-propagation fold occurred during this time, as can be observed from the plot of cumulative shortening versus geological age (Fig. 5g). The restoration to early Cretaceous time (97 Ma) shows the regional dip of the Top Muschelkalk surface remained towards the ESE. The early Cretaceous rocks also thicken in this direction. Minor WNW-trending folds also remain present in the Muschelkalk surface as well (Figs. 5e and 6e).

The restoration representing earliest Cretaceous times (146 Ma) shows the Top Muschelkalk surface with a change in the regional dip to the NE (Figs. 5f and 6f) and with the Keuper unit thickening to the NE (Fig. 5f). In addition to the regional dip, the Top Muschelkalk surface is also deformed by two minor, broad folds that trend between WNW and NW. In the final restoration in the sequence (not shown), the Top Muschelkalk surface was flexurally unfolded to a horizontal target surface to act as a reference for the shortening and area-based strain analyses.

The loose lines for the cross-sections that have been extracted from the 3-D model at each restoration stage show very little deformation (Fig. 5). However, the map-view loose lines along the southern margin of the Top Muschelkalk surface at each restoration stage provide more information about the variability of horizontal shortening across the area (Fig. 7; shortening was measured across the surface in the maximum shortening direction).

The unfolding direction and the shortening measurement are oblique to the 3-D model boundaries, which reduces the amount of apparent shortening in the SE and NW corners of the model (Fig. 7a) because the anticline is not intersected in the unfolding direction (Fig. 7b; at approximately 6300 m along the E–W axis). The Top Muschelkalk surface loose lines show a general apparent increase in shortening from east to west from approximately 250 to 590 m (Fig. 7a and b). This increase is a minimum shortening, however, as some of the minor folds are not represented across the whole model (e.g. the present-day southern limb of the southern syncline is not included).

Once the coverage has been taken into account, the local variability in shortening reflects real changes in fold geometry that might be produced by displacement or geometry changes along strike of the fault. Large, local distortions of the loose line that reflect changes in the amount of local shortening should be examined in more detail (e.g. the local increase in shortening seen between 0 and 750 m; Fig. 7b). These areas of anomalous deformation of the map-view loose line may represent zones of increased local deformation or may highlight areas where the interpretation requires adjustment. In either case, these regions are more easily recognised and adjusted with 3-D restorations in contrast to 2-D restorations.

The change in surface area of the Top Muschelkalk surface has been determined at each restoration stage (Fig. 7c). The actual surface area of the Top Muschelkalk surface is interpreted to have decreased from the mid Triassic to the present-day based on the restorations, with the greatest magnitude of change occurring during the Cretaceous. Hennings et al. (2000) noted that surface-area changes produced by plane-strain flexural-slip unfolding of a surface represent the deviation of the fold shape from a constant-amplitude, cylindrical fold. In this restoration, the area change of the Top Muschelkalk is a product of the non-cylindrical nature of the structure, the compaction of the sedimentary sequence through time, and the non-parallel geometry of the layers. Area strains generated by using a slip system parallel to the uppermost (template) surface at each restoration stage relate not only to the local angular deviation between the template surface and the target surface, but also to the angular deviation of the passive surfaces and the slip system.

In summary, the restorations bracket the contractional phase of the structure to the late Cretaceous, with only minor regional tilting during other stages. Fig. 5g shows that the rate of shortening sharply increased from the late Triassic and early Cretaceous regional tilting to the active thrusting and folding of the late Cretaceous. The amount of contraction decreased during the Maastrichtian and did not continue into the Tertiary. Other studies across the entire NW German Basin show abundant evidence that the contraction phase started no earlier than the onset of the late Cretaceous Coniac stage (88 ma according to Harland et al., 1989), and lasted through the Coniacian–Santonian and partly into the Campanian and Maastrichtian (Baldschuhn et al., 1991, and references therein). Our analyses do not have enough resolution to precisely establish the onset of the contractional phase, because the seismic interpretation has not discriminated the Coniacian from the early Cretaceous or Santonian intervals. Even so, application of this new restoration technique to this structure described above has produced results that are in agreement with the regional geohistory already established.

4. Conclusions

A new, robust technique for 3-D restoration of flexural-slip folds has been presented. This plane-strain technique preserves volume between folded layers, orthogonal thickness of layers and line length in the unfolding direction of layers parallel to the template surface, whilst maintaining the folded object topology. An important advantage of this algorithm over previously published techniques is that restoration of multiple, geometrically complex, and non-parallel surfaces is possible in a single modelling increment. This 3-D technique also represents a significant advance over 2-D approaches. Specifically, a single 2-D restoration does not sufficiently constrain the interpretation in the third dimension. Alternatively, multiple serial 2-D restorations are time-consuming to create and frequently result in incompatibilities between individual sections.

A 3-D model of a salt-cored, fault-propagation fold has been sequentially restored using this technique. We first

determined that the shortening direction for the fold was approximately N–S (189°) by analysing the unfolding strains. The restorations suggest that the fold initiated during late Cretaceous times with shortening and fold amplification ceasing by Tertiary times. The use of map-view loose lines in the 3-D restorations help to identify geometric problem areas in the model or regions that have experienced more intense deformation. The timing of fold development (and by inference the initiation of regional compression during the late Cretaceous) determined from the restorations agrees with published interpretation for the initiation of shortening in NW Germany.

Acknowledgements

The authors would like to thank BEB and Exxon/Mobil for access to, and permission to use, the 3-D geological model of the German fold. The modelling environment and the implementation of the algorithm have been carried out using Midland Valley's 3DMove software. Mark Cooper, an anonymous reviewer and Scott Wilkerson provided thorough reviews that greatly improved the scientific content and readability of the manuscript.

References

Allen, P.A., Allen, J.R., 1990. Basin Analysis, Principles and Applications. Blackwell Science, Oxford.

Baldschuhn, R., Best, G., Kockel, F., 1991. Inversion tectonics in the north-west German basin. In: Spencer, A.M. (Eds.), Generation, Accumulation, and Production of Europe's Hydrocarbons. Special Publication of the European Association of Petroleum Geologists 1, pp. 149–159.

Geiser, J., Geiser, P.A., Kligfield, R., Ratliff, R., Rowan, M., 1988. New applications of computer-based section construction: strain analysis, local balancing, and subsurface fault prediction. The Mountain Geologist 25, 47–59.

Gratier, J.-P., Guillier, B., 1993. Compatibility constraints on folded and faulted strata and calculation of total displacement using computational restoration (UNFOLD program). Journal of Structural Geology 15, 391–402.

Gratier, J.-P., Guillier, B., Delorme, A., Odonne, F., 1991. Restoration and balance of a folded and faulted surface by best-fitting of finite elements: principle and applications. Journal of Structural Geology 13, 111–115.

Harland, W.B., Armstrong, R.L., Cox, A.V., Craig, L.E., Smith, A.G., Smith, D.G., 1989. A Geologic Time Scale. Cambridge University Press, Cambridge.

Hennings, P.H., Olson, J.E., Thompson, L.B., 2000. Combining outcrop data and three-dimensional structural models to characterize fractured reservoirs: an example from Wyoming. American Association of Petroleum Geologists Bulletin 84, 830–849.

Kockel, F., Wehner, H., Gerling, P., 1994. Petroleum systems of the Lower Saxony Basin, Germany. In: Magoon, L.B., Dow, W.G. (Eds.), The Petroleum System—from Source to Trap. American Association of Petroleum Geologists Memoir, 60, pp. 573–586.

Leger, M., Thibaut, M., Gratier, J.-P., Morvan, J.-M., 1997. A least-squares method for multisurface unfolding. Journal of Structural Geology 19, 735–743.

Ramsay, J.G., Huber, M., 1987. The Techniques of Modern Structural Geology. Volume 2: Folds and Fractures. Academic Press, London.

Rouby, D., Xiao, H., Suppe, J., 2000. 3-D restoration of complexly folded and faulted surfaces using multiple unfolding mechanisms. American Association of Petroleum Geologists Bulletin 84, 805–829.

Williams, G.D., Kane, S.J., Buddin, T.S., Richards, A.J., 1997. Restoration and balance of complex folded and faulted rock volumes: flexural flattening, jigsaw fitting and decompaction in three dimensions. Tectonophysics 273, 203–218.